# Design of a test rig for the characterization of friction and wear in hot-metal gas-forming of AA 5083 aluminium sheets

International Journal of Lightweight Materials and Manufacture 8 (2025) 241–251

Contents lists available at ScienceDirect

International Journal of Lightweight Materials and Manufacture

journal homepage: www.keaipublishing.com/ijlmm

# Design of a test rig for the characterization of friction and wear in hot-metal gas-forming of AA 5083 aluminium sheets

Federico Simone Gobber [a, *], Alexandru Tancau [a], Leonardo Daniele Scintilla [b], Marco Fontana [b], Marco Actis Grande [a]

[a] Politecnico di Torino - Dept. of Applied Science and Technology (DISAT), C.so Duca degli Abruzzi 24, 10129 Torino, Italy
[b] Fontana Pietro SpA, Viale Alcide De Gasperi 16, 23800 Calolziocorte, LC, Italy

ARTICLE INFO

*Article history:*
Received 28 February 2024
Received in revised form
7 July 2024
Accepted 5 September 2024
Available online 18 September 2024

*Keywords:*
Superplastic-forming
5083 aluminum alloy
Friction
Lubrication

ABSTRACT

Advanced aluminium sheet-forming processes such as the hot-metal gas-forming represent a challenging solution for producing small lots in the high-end car bodies industry, and the adoption of single cavity moulds made from low-cost, easily machinable materials such as cast iron reduces the overall sheet-forming costs. The tribological properties of the mould-sheet tribopair are of great interest for optimizing the sheet forming obtaining an acceptable esthetic surface finishing. This study presents the design and construction of a lab-scale experimental test rig for the tribological characterization at high temperatures of the mould-sheet tribopair. The proposed test method reproduces the sliding at the mould-sheet interface with contemporary sheet straining up to $\varepsilon = 0.8$ at strain rates in the $1.2*10^{-3}$ to $2*10^{-2}$ $s^{-1}$ range. A series of experiments were carried out in dry and lubricated conditions for a ductile iron EN-GJS grade sliding against a AA 5083 aluminium alloy while straining. After comparing the experimental results with the literature data from other test rigs, comparable results were obtained as COF regards, ranging between 1.2 and 2.5 in dry sliding and between 0.05 and 0.2 in lubricated sliding. The morphological characterization of the sliding surfaces and cross-sections highlights the strong tendency to galling in dry sliding conditions expecially for low strain rates.


## 1. Introduction

Within the hot-forming processes of aluminium alloys, some materials are traditionally used to manufacture forming tools, such as dies and punches. Typically, steels, specifically hot-working steels, are widely used in plastic deformation or casting processes of aluminium alloys. However, metal-forming processes such as hot-metal gas-forming have few similarities to other sheet metal forming processes (e.g. cold stamping, hot stamping, deep drawing) and are characterized by a high complexity of the achievable shapes [1]. In addition, the dies used in hot-metal gas-forming are large, and their surface finishing must be strictly controlled to produce parts suitable for painting. The interaction between the die and sheet metal is a significant issue contributing to sheet metal damage during the forming process, leading to the formation of defects on the painted surface, such as the so-called orange peel. Therefore, a proper selection of the die design [2] and material [3] is crucial to maximizing process efficiency and must be referred to guiding parameters such as processability, polishability and microstructural stability at high temperatures. Lubrication is always required to lower the interfacial shear strength and avoid direct contact between the interacting surfaces [4], to promote low friction and wear when forming aluminium. However, lubricants can fail, and significant issues with material transfer arise or even worse, necking can occur when lubricant quantity is exceeded [5]. Because of this, interruptions are needed for tool refurbishing; this issue affects process efficiency. In hot-metal gas-forming (HMGF), wear on both the tool and the aluminium sheet surfaces is severely influenced by the characteristic process parameters [5]:

- The high average temperature on the die (400–500 °C);
- The high friction between the aluminium alloy sheet and the die, typically made of a ferrous alloy (steel or cast iron), that

* Corresponding author.
*E-mail address:* federico.gobber@polito.it (F.S. Gobber).
Peer review under responsibility of Editorial Board of International Journal of Lightweight Materials and Manufacture

https://doi.org/10.1016/j.ijlmm.2024.09.002

occurs for prolonged times and with intimate contact between the surfaces.

In HMGF processes involving aluminum alloys, wear and friction are particularly critical due to the distinct characteristics of aluminum at elevated temperatures. Aluminum alloys, often used for their excellent strength-to-weight ratio [6–9], become significantly softer and more ductile at the high temperatures employed in HMGF, typically around 500–600 °C. This softening increases the propensity for aluminum to adhere to the tool surfaces, leading to severe sticking and galling. Furthermore, the high thermal conductivity of aluminum alloys exacerbates the heat transfer to the forming tools, accelerating wear and degradation. The high pressures required in HMGF amplify the frictional forces between the aluminum alloy workpiece and the tool, intensifying abrasive wear. As the fundamental wear mechanisms regard (adhesive wear, abrasive wear, triboxidative wear, surface fatigue wear), high temperature and very low sliding speeds between the die and the aluminium sheet (deformation speed of the sheet $10^{-5}$ - $10^{-3}$ $s^{-1}$) contribute synergistically to adhesive and triboxidative wear mechanisms. A solid lubricant interposed between the die and the sheet (e.g. $MoS_2$, BN or graphite) is essential to preserve both the die and the sheet, preventing surface seizure; however, as reported by Ref. [10], hard abrasive particles may originate from the interaction between the iron contained in steels or cast iron and the aluminium contained in the sheet despite adopting a solid lubricant, due to galling mechanisms. Once the forming operation is complete, such hard particles may adhere to the die surface and damage the next sheet formed.

### 1.1. Wear and friction characterization

In the frame of hot-metal gas-forming techniques, several processes exploiting the superplastic properties of the sheets to deform are documented in the literature, being known as superplastic forming (SPF) [10], quick plastic forming (QPF) [11] and more recently hot form quenching (HFQ) [12]. Furthermore, applying innovative surface treatments on hot-metal gas-forming dies by adopting plasma-deposited self-lubricating coatings such as WC/C [13] with a duplex treatment strategy [14,15] gave promising results in improving the frictional properties and reducing the use of solid lubricants. Nevertheless, treating dies as large as those employed in hot-metal gas-forming for automotive in CA-PVD chambers is not feasible on a broad scale despite significant reduction of aluminum transfer at high temperature [16]. The direct evidence of wear and frictional outcomes can be observed on dies and sheets right after forming: the analysis of an aluminium sheet can be carried out at a relatively affordable cost, focussing on R&D purposes; on the other hand, this is not true when it comes to analyzing the surface of a large die. For this reason, since hot-metal gas-forming techniques were established at the production level, studies on high-temperature friction and wear in the die-sheet tribopair have been carried out and documented in the literature.

While Liu et al. [17] have thoroughly described the literature regarding test rigs for the hot-forming of aluminium alloys, no critical description was found by the authors for test rigs specific for hot-metal gas-forming. The research on the process has led to the development of ad-hoc formability tests (i.e. bulge test [18]), but very little literature has investigated the tribological interaction between the aluminium sheet and the die. The most straightforward approach to evaluate tribological properties accounting for high temperature and loading is using a conventional flat-on-flat reciprocating sliding tribometer modified according to Hanna [19] to represent the aluminium sheet-to-die contact better. Such an approach is accurate and relatively straightforward as configuration regards but does not include the effect of the deformation acting on the aluminium sheet; in Ref. [19], it is the die-like sample that slides on the aluminium sheet while the hot-metal gas-forming processes work on the opposite principle. Another test rig specific for superplastic forming was developed by Friedman et al. [20]; similarly to Ref. [19], also this test adopts a flat-on-flat configuration of the sliding surfaces with an aluminium sheet sample fixed on a horizontal plane and the block representing the die that is moved by an actuator. Even this test rig does not account for the effect of the deforming sheet, but the tribopair is more uniformly heated by enclosing it in an oven. Recently Rodriguez Leal et al. [21] developed a similar test based on reciprocating sliding but limited the maximum test temperature to 300 °C which is rather low compared to the operational ones. Interestingly they focused their research on the role of the lubricant in SPF and dedicated a consistent part of their study to its cleanability from the mould surface.

The most accurate configuration of a test rig simulating the sheet-to-die contact in hot-metal gas-forming is that developed by Das et al. [22]; in this test rig, the aluminium sheet is provided as a coil, and the die material is represented as a pin. The coil is unwound from a pulley at a certain speed while it is wound on another pulley travelling at a higher speed; thus, the aluminium sheet deforms at a rate related to the velocity ratio. At a mid-distance between the two pulleys, the sheet slides on a heated roller painted with lubricant; on the opposite side of the roller, a pin made of the die material slides on the aluminium sheet. The pin is normally loaded with a static weight while a load cell measures the resultant tangential force enabling the calculation of the coefficient of friction (COF). The contact is non-conformal, with a flat surface (aluminium sheet) sliding against the lateral surface of a cylinder (pin). Despite accounting for the different mechanisms occurring during hot-metal gas-forming, this test rig has a large footprint and needs to manufacture specific aluminium coils to perform the test. Moreover, the heating control can be challenging to manage due to the non-uniform heating sources.

The comparison of dry and lubricated testing in SPF represents a considerable challenge since, as pointed out by the literature on the topic [3] many factors can play an active role in the tribological problem: dry sliding at high temperature results in instantaneous adhesion and consequently high friction making the test non representative of the real working conditions; the lubricant choice can modify the tribological mechanisms based on its degradation (e.g. polymeric lubricants) or poor adhesion (e.g. hBN), furthermore even the die surface finishing represent a factor to keep under control since even mirror polished surfaces can scratch the aluminum sheet when carbides are protruding.

A comprehensive approach to this tribological problem has been proposed by Morales and colleagues, yet the tribometer, despite its high degree of representativeness in terms of reproducible stresses and temperatures, is a complex apparatus requiring the use of an entire coil of aluminium sheet for testing. Based on the above-mentioned considerations, the present study proposes a lab-scale configuration tribometer for testing materials employed in hot-metal gas-forming. The approach of the test rig presented in this paper aims at filling the shortcomings in the literature regarding a tribotesting unit able to reproduce the main mechanisms of wear and friction encountered in aluminum SPF in a compact unit, capable of reaching high temperature. After describing the design criteria adopted, the results from dry and lubricated testing are compared in terms of COF and surface morphology of the tribopair for some near-process selected conditions.

## 2. Test-rig design and adjustable parameters

The test-rig design was based on the high-temperature testing requirements, as shown in Fig. 1. In principle, the test is resumable as a high-temperature tensile straining of an aluminium sheet sample, causing sliding at the interface with a cube placed on top of it. The core of the rig is a 3 kW tubular furnace with ceramic liners capable of reaching up to 900 °C (1). A sample holder made of AISI 309 austenitic stainless steel (7b) is mounted inside the furnace to fix an aluminium sheet sample (5) for tensile testing with a gauged length of 50.0 ± 0.1 mm (Fig. 1d). AISI 309 steel grade was selected due to its high resistance to oxidation at high temperature; in fact, it is considered a heat-resistant grade and is commonly employed in the manufacture of furnace parts, heat exchangers and parts for service at high temperature. The mechanical properties of AISI 309 and the size of the sample holders ensure that it will be the aluminium alloy sheet to deform during the test at high temperature. The tubular furnace is open at both ends and set by a controller fitted with a K-type thermocouple placed below 7b, close to the aluminium sheet sample. The aluminium sample is strained by a stepper motor (3) rigidly bound to the aluminium sample by an upper sheet holder (7a).

While the aluminium sheet strains, a cast iron block (4) (20 × 20 × 15 mm) is placed on top and screwed to a sample holding bar (6), and similarly to Ref. [19], the flat-on-flat condition is guaranteed throughout the testing by a spherical joint between (6) and (4). The deformation resulting from straining is measured by tracking the displacement of control points on the strained sample. Each control point is marked before testing the unstrained sample at 5 mm intervals. Due to the sample holding bar's proper weight, a minimum normal load of 5.6 N acts on the contact area during the test; nevertheless, it can be increased by adding calibrated weights to a pin at a half-length of (6). In addition, the total contact area can be modified based on the sample's geometry: those reported in Fig. 1c and d have a total contact area of 100 $mm^2$.

On the left side of Fig. 1a, the stepper motor controlled by an NI PCI 6503 board operates the stretching of the aluminium sheet outside the furnace while at high temperature; on the right side of Fig. 1a—a load cell recording forces in the 0.1–250 N range detects the tangential force developed at the sheet-mould contact and sends the data to the controller board. The input data (test parameters) are managed by a program compiled in the Labview environment, and output data (tangential force values) sampled every 0.1 s are saved to a spreadsheet file for the subsequent filtering and data treatment. The maximum displacement achievable by the rig is 40 mm; such displacement is equivalent to $\varepsilon = 0.8$ for the sample of Fig. 1d after eq. (1). A range of deformation rates characteristic of hot-metal gas-forming can be explored by tuning the stepper motor linear velocity from 1 up to 100 mm/min in the $4*10^{-4}$ to $2*10^{-2}$ $s^{-1}$ range after eq. (2).

$$\varepsilon = \frac{\Delta L}{L_0} \quad \text{Eq.1}$$

$$\dot{\varepsilon} = \frac{d\varepsilon}{dt} = \frac{v}{\Delta L} \quad \text{Eq.2}$$

The motivations for adopting the proposed configuration lie in the process, more specifically, due to the reproducibility of specific sliding conditions encountered in the hot-metal gas-forming (Fig. 2). At first, when the hot metal sheet starts deforming due to the gas pressure, a limited area touches the mould; a so-called free-expansion regime characterizes the first phase of deformation (Fig. 2a), where most of the friction is exerted closely to the blank holder by the first parts of the sheet touching the mould. Similarly, the proposed test-rig configuration precisely reproduces the

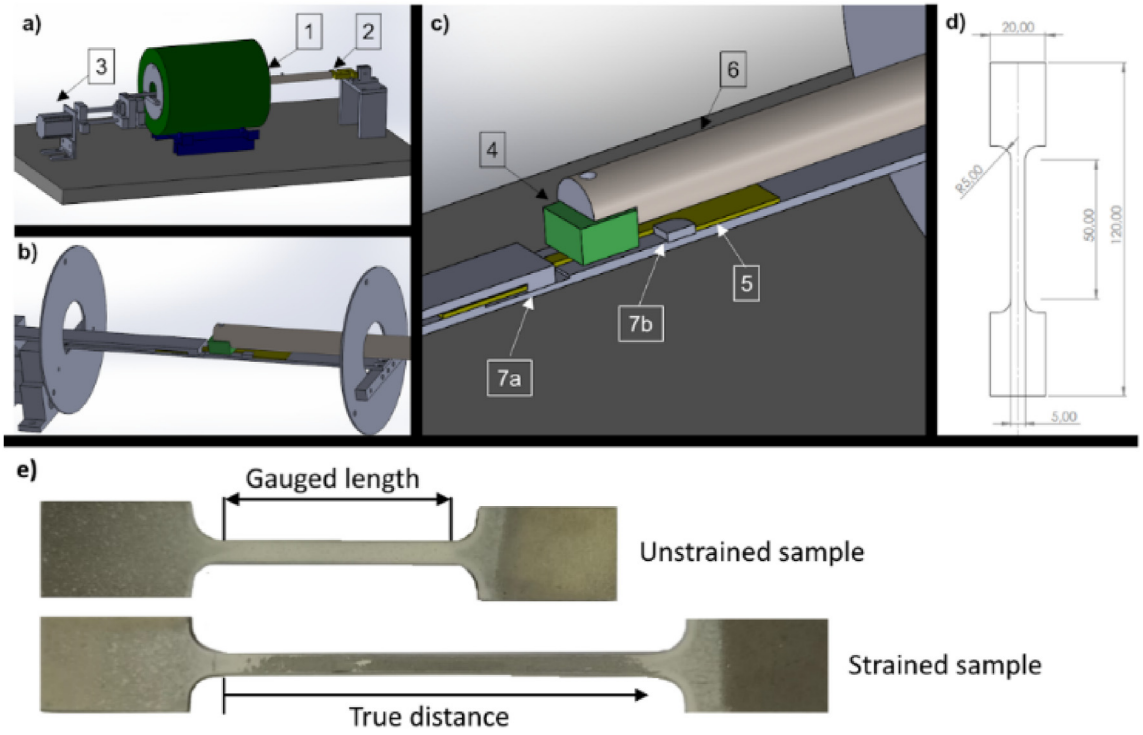


**Fig. 1.** 3D model of the test rig and schematics of the samples. a) general overview of the test rig with (1) furnace, (2) load cell and (3) stepper motor. b) insight into the testing system. c) close-up of the tribo-contact area with (4) die-representing coupon, (5) aluminium sheet sample, (6) sample holding bar, (7a) upper sheet holder and (7b) lower sheet holder. d) schematics of the tensile testing sample made from AA 5083 1.5 mm thick aluminium sheet. e) sample prior and after testing.

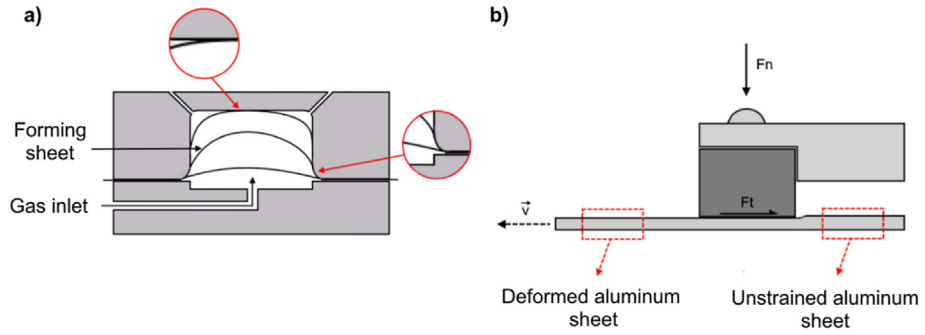


**Fig. 2.** Schematics represent the frictional characteristics in the hot-metal gas-forming process adapted from Ref. [27] a) and the test rig presented in this study b).

aluminium sheet-mould tribopair sliding condition in the proximity of the blank holder. In this case, the aluminium sheet is deformed uniaxially at a constant velocity and friction results from applying a normal load on the mould-like sample (Fig. 2b). With increasing forming time, the sheet starts copying the mould's complex surface: consequently, the portions of the aluminium sheet, previously freely expanded, touch the mould surface. If dry sliding conditions are considered, the sheet surface after the free expansion differs from the undeformed one due to the modification of aluminium's surface oxide layer and its frictional behaviour [23,24]. The tribology in lubricated conditions as experienced by the production process is currently debated. The frictional behaviour due to the sheet-mould mechanical interaction located at the asperities [25] increases as the thickness of the solid lubricant decreases; such a thinning reduces the number of lubricant particles effective in limiting the metal-metal contact at the asperities of the sheet-mould interface. An up-to-date overview of the literature regarding this topic is given in Ref. [26]. In principle, the proposed test rig can reproduce these tribological conditions by employing pre-strained sheet samples representative of the deformation rate reached by the sheet when touching the mould in a specific area. Nevertheless, this topic is considered out of this article's scope, aiming mainly to validate the proposed testing method by comparing it to consolidated results from the literature.

## 3. Materials

The two materials chosen for producing the samples representing the mould and the aluminium sheet are ductile iron EN-GJS grade as the mould material regards (composition reported in Table 1) and a 1.5 mm thick sheet of AA 5083 aluminium alloy (composition reported in Table 2), specific for superplastic forming applications, in heavily cold-rolled state. The superplastic behaviour is guaranteed by the very fine grains (less than 10 μm) that are formed thanks to the cold rolling process. In fact at high temperature these microstructures are highly susceptible to creep deformation, allowing remarkable elongation to be achieved. Ductile iron was chosen since it is used in the manufacture of industrial SPF moulds, thanks to its low cost and high mechanical workability. The small samples cut by an abrasive disc and then milled to the final dimensions. The surface was prepared by using grinding SiC papers for metallographic preparation. All samples were ground using grits from 200 to 1200, to reach a final average surface roughness (Ra) of 0.03 μm (measured by roughness tester Hommelwerke T1000), comparable to that of the real mould. The choice of cast iron, apart from the low materials cost, can have some interesting characteristic as the presence of graphite nodules may act themself as an embedded solid state lubricant. On the other hand the graphitic domain could represent a weak region that may wear out early when sliding at high temperatures.

In addition, cast iron is widely employed in manufacturing large moulds due to its good machinability, low cost and metallurgical stability at the processing temperature (400–500 °C). On the contrary, the low intrinsic hardness (225 ± 4 $HV_{10}$) of its microstructure constituted by perlite and graphite nodules (Fig. 3a) does not favour the die polishability. Furthermore, as reported in the literature, the AA 5083 is a non heat-treatable alloy constituted by an aluminium-rich matrix with dispersed $Al_6Mn$ intermetallics. Rolling-induced cracks on the surface oxidized layers were observed in the as-rolled condition for the material used in this study, as also documented in Ref. [22] for the same aluminium alloy in comparable metallurgical conditions (as-rolled) (Fig. 3b).

**Table 1**
Chemical composition of the ductile iron employed to manufacture the samples.

| | C [%wt] | Si [%wt] | Mn [%wt] | S [%wt] | P [%wt] | Fe [%wt] |
|---|---|---|---|---|---|---|
| EN-GJS | 3.51 | 2.72 | 0.21 | 0.01 | 0.004 | Bal. |

**Table 2**
Chemical composition of the AA 5083 aluminium alloy employed to manufacture the samples.

| | Mg [%wt] | Mn [%wt] | Cr [%wt] | Fe [%wt] | Si [%wt] | Al [%wt] |
|---|---|---|---|---|---|---|
| EN-AA 5083 | 4.53 | 0.71 | 0.12 | 0.08 | 0.03 | Bal. |

## 4. Experimental procedure

### 4.1. Continuous sliding tests

Each condition reported in Table 3 was tested five times on samples with the geometry of Figs. 1d and 1.3 mm thickness to reproduce tests comparable to those found in the literature for dry [22] and lubricated conditions [19]. The deformation rates were selected to align with the specific characteristics of the process being replicated by this test rig configuration. As previously reported, this test rig configuration is designed to reproduce the tribological interaction that occurs when the initial portions of aluminium sheet contact the mould. Therefore, the high strain rates characteristic of the free inflation part of the process were selected. The experiments were performed randomly to mitigate the effect of the experimental error. Once the furnace reached 500 °C, the aluminium sheet sample was introduced and let soak for 5 min to ensure a proper temperature homogenization; then, the cast-iron block was placed on top and loaded with 8.6 N to reproduce a pressure close to 1 bar. The simulated conditions reproduce the sheet-die sliding of a portion of the sheet touching the die surface when the process begins, and no considerable strain has occurred to the sheet yet. Such a condition is representative of portions of the aluminium sheet close to the blank holder.

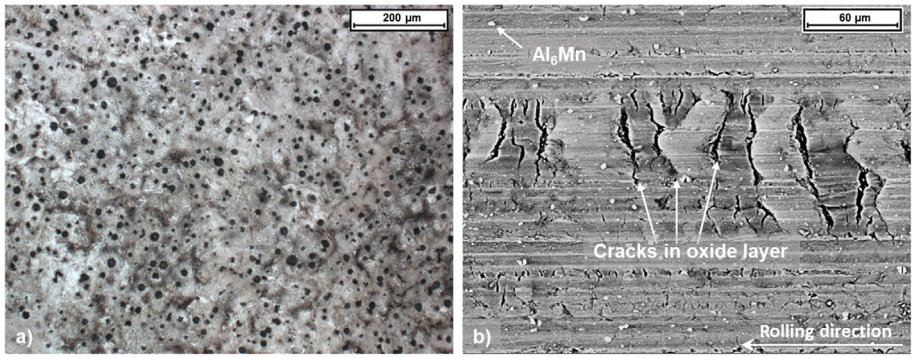


**Fig. 3.** Microstructures of the starting materials: a) optical micrograph of an EN-GJS, b) SE - SEM micrograph of a AA 5083 sheet sample.

**Table 3**
Experimental parameters for dry and lubricated tests made under a continuous sliding regime.

| | Sliding distance [mm] | Sliding speed [mm/min] | $\dot{\varepsilon}$ [$s^{-1}$] | Load [bar] | Lubrication |
|---|---|---|---|---|---|
| G3 | 40 | 3 | $1.2 * 10^{-3}$ | ≈1 | Dry |
| G30 | | 30 | $1.2 * 10^{-2}$ | | Dry |
| G50 | | 50 | $2.1 * 10^{-2}$ | | Dry |
| G100 | | 100 | $4.2 * 10^{-2}$ | | Dry |
| GL_3 | | 3 | $1.2 * 10^{-3}$ | | BN |
| GL_100 | | 100 | $4.2 * 10^{-2}$ | | BN |

The cast-iron coupons were polished to mimic the surface finishing of approximately 0.03 ± 0.02 µm (Ra) measured experimentally on industrial moulds. The surface of the coupons was prepared using an automated orbital metallographic polishing machine (Presi Mecatech 250 SPI). Four samples were mounted on the polishing machine for each run, and the final texture was completely random, lacking any preferential orientation of scratches.

At the end of the test, both the sheet and the mould sample were inspected. The elongation along the gauged length was determined by comparing the deformation of six control points marked on the rear of each sample before performing the test at a distance of 10 mm from each other. The thickness of each sample was measured with a micrometre after the test for each condition. Morphological analysis was performed through stereomicrographs (Leica mod. M5S) and Scanning Electron Microscopy (SEM – Zeiss EVO 15 equipped with secondary and backscattered electron probes). In addition, the presence of tribolayers and the composition of transferred layers were assessed by Energy Dispersive Spectroscopy (EDS – Oxford Ultim Max). One sample per each condition was cut in half, mounted in epoxy resin, and prepared metallographically to observe the cross-section by light optical and scanning electron microscopes. When necessary, cross-sectioned samples were etched with Keller etchant [28] before observation with the light optical microscope. Both SEM imaging and EDS analysis were performed with 20 kV acceleration voltage, 8.5 mm working distance, 45 s acquisition time and 400 nm spot size.

## 5. Results and discussion

The difference between dry and lubricated sliding conditions is highlighted macroscopically in Fig. 4, with both scratches and transferred material detectable on the surface of dry-tested samples. Conversely, the lubricant paint protects the surface of the lubricated samples, so no thick debris layers or transferred material are detectable. Considering dry samples more in detail, a relevant and non-uniform shrinkage is revealed for the samples strained at 3 mm/min leading to the sample's rupture at the end of the test. In addition, consistent voids were formed during straining, highlighted by the red circle in Fig. 6, with the rupture occurring due to their coalescence. An abrupt variation in thickness for sample 3 is located at the entrance of the contact region, where the deforming aluminum sheet sample starts sliding against the cast-iron cube. The red arrows in Fig. 6 point to the cube's edge for each testing condition. Further to the samples tested at 3 mm/min, straining at 100 mm/min in dry-sliding conditions also resulted in sample rupture but closer to the centre of the sample, out of the cube area, while samples strained at 3 mm/min broke under the cube area.

Intermediate straining rates (30 and 50 mm/min) resulted in a more homogeneous deformation of the aluminum sheet sample along the gauged length. Despite debris and scratches still being evident (Fig. 4), the step-like separation between the region prior and that under the cube is challenging to observe qualitatively from micrographs (Fig. 5). The cross-sectioned surface appears rougher for the dry samples in the area close to the red arrows, while a smoother surface is characteristic of lubricated samples. Nevertheless, even lubricated samples are not defect-free, and scratches are detectable from stereomicrographs (Fig. 4); this characteristic is representative of superplastic-formed sheets, and similar surfaces are documented in the literature [29,30]. Considering deformations (Fig. 6), significant differences emerge for tests carried out under lubricated or dry conditions. The deformation tends to be more uniform along the sample length as the coefficient of friction decreases and under specific ratios between friction and straining. Altogether the sample length increases by 80% along the gauged length, but such deformation is not homogeneous, as observed in Fig. 7b. Similar considerations are proposed regarding thickness. In Fig. 7a, the final thickness is represented against the true distance, meaning the distance each control point has been displaced due to straining.

The thickness along the deformed aluminium sheet is relatively uniform for lubricated samples, between 1.16 ± 0.08 mm, independently from the strain rate. A more pronounced relation between strain rate and thickness reduction emerges for dry sliding. Conversely, in Fig. 6b, the displacement of each control point calculated to its undeformed position is represented against its

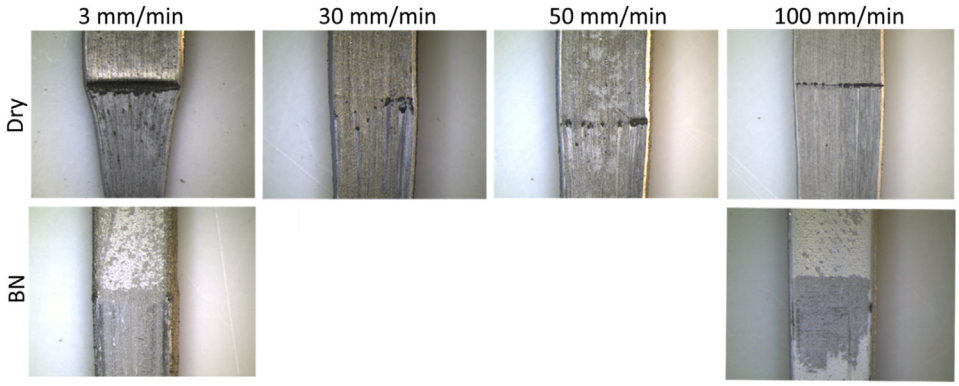


**Fig. 4.** Stereomicrograph of the tested AA 5083 samples highlighting the wear tracks close to the cube block.

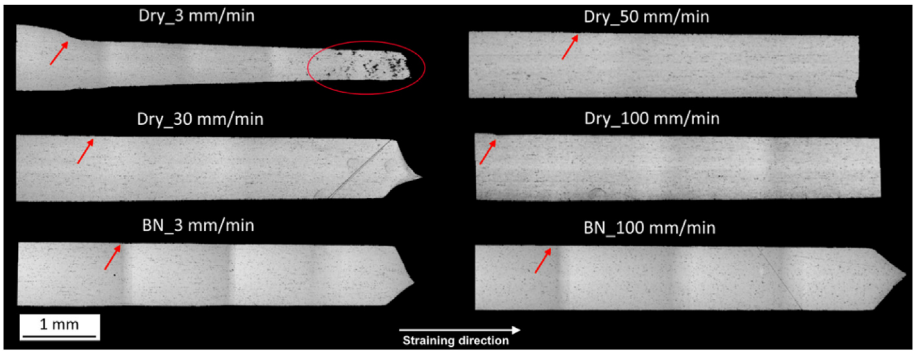


**Fig. 5.** Metallographic cross-sections of the stretched aluminum sheets.

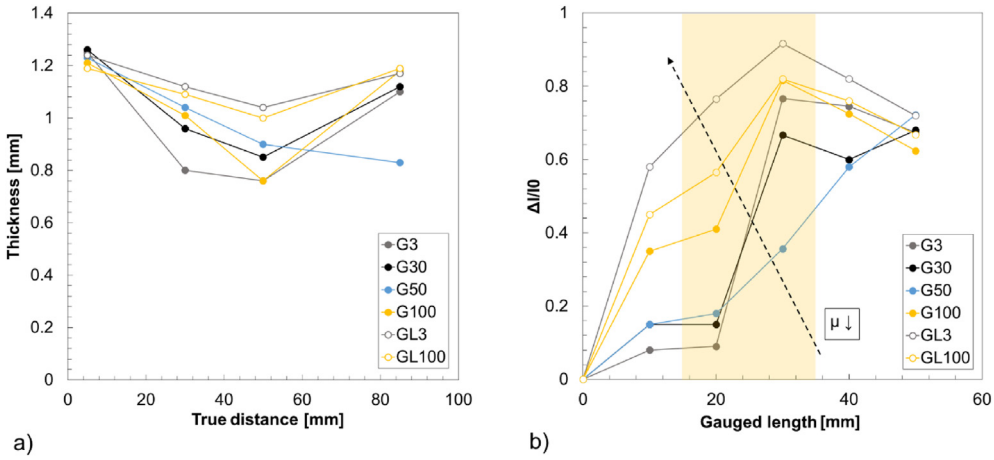


**Fig. 6.** Dimensional variations in the deformed samples. a) thickness variation along the straining direction, b) elongation along the gauged length.

undeformed position along the gauged length. The yellow region represents the area along the gauged length where the cast-iron cube is placed, with the left boundary of this region corresponding to the red arrows in Fig. 5. In Fig. 6a, the different locations of thinning between the two dry-sliding conditions leading to sheet rupture (3 mm/min and 100 mm/min) are reported. For all the tested strain rates, the cube acts as a barrier to deformation whether the aluminum sheet is dry or lubricated. Such a condition can represent the sliding regime of those sheet regions surrounding the first areas touching the mould during a superplastic forming. The cube's blocking action is more easily visible in Fig. 6b.

In dry sliding, the cube hiders the portions of the sheet it is lying on to deform freely, much more than in lubricated sliding. For this reason, the control points falling in the yellow area have lower deformation; the deformation of those points placed at the entrance to the contact is slowed down, and the strain decreases consequently.

Based on the previous observations, separate considerations and hypotheses can be inferred for each strain rate under dry sliding:

−3 mm/min corresponding to $\dot{\varepsilon} = 1.2{*}10^{-3}$ is a low strain rate rarely tested in the literature under lubricated conditions [25], while no data are available for dry sliding. Therefore, the time

required for the aluminum sheet to deform and exit the contact area is high. Conversely, there is plenty of time for adhesion mechanisms to take place. In addition, the Iron contained in the cast-iron cube, and the Aluminum from the sheet have high tribological compatibility, meaning there is a strong tendency to form AlFe-based intermetallic compounds [31] leading to welded joints. This mechanism is responsible for severe galling between the two surfaces [32]. Furthermore, the aluminium alloy is very soft at 500 °C, so it can deform and plough easily, its section decreases due to plastic deformation under the cube load, and intimate contact between the surface asperities is likely to occur. If the adhesion between the two surfaces is strong enough, the cube acts as an obstacle to deformation, constraining the sheet and reducing the portion able to deform to about half the total gauged length. As a result, deformation is localized, and the aluminum sample breaks after necking. Another indication that normal-load thinning is relevant relates to the point where rupture occurs, immediately at the cube front.

- at 30 and 50 mm/min, corresponding to $\dot{\varepsilon} = 1.2*10^{-2}$ and $\dot{\varepsilon} = 2.1*10^{-2}$, the amount of sliding at the cube/sheet interface and the sheet deformation are balanced. The cube is not blocking the material from deforming, as confirmed by the absence of steps in the micrograph of Fig. 6, but it still exerts pressure and slows the deformation. The coefficient of friction is lower than the G3 sample, resulting in an evenly and more linearly deformed sheet. The cube still does not accommodate the homogeneous deformation and resistance to sliding.

- at 100 mm/min, corresponding to $\dot{\varepsilon} = 4.2*10^{-2}$ the sheet breaks due to an unbalanced amount of deformation and a high coefficient of friction, which cannot deform without lubrication. As literature regards, this strain rate is still low in free-forming conditions [33], but when sliding against the cube surface, further contributions to deformation has to be considered, such as the load-related thinning contribution. The coefficient of friction is still comparable to the 30 and 50 mm/min tests, but rupture occurs similarly to the 3 mm/min deformation rate. At 100 mm/min, the material still slides under the cube load, which is not blocking the sheet. The relatively high coefficient of friction causes the sheet to strain at a variable rate along the gauged length. Where the mismatch between the strain rates and deformations exceeds the material limits, the sheet slides and deforms under the cube at a much lower rate than the sheet just deformed downstream of the cube.

As lubricated sliding regards, the tests performed at 3 and 100 mm/min under lubricated conditions validate the hypothesis on dry sliding. After a substantial friction reduction at the cube/sheet interface, the deformation rate is more evenly distributed along the sample length. As a result, the sheet deforms without breaking even at those strain rates causing rupture under dry sliding.

The different friction coefficients (Cof) are reported in Fig. 7 for each tested condition. Considering dry Cof first, a further indication of how deformation and sliding concurred is appreciable. The Cof for the very low strain rate ($1.2*10^{-3}$ $s^{-1}$, 3 mm/min) is not realistic but is reported for completeness and to explain the test outcome. Its average value is significantly higher than all the other Cof in dry sliding, and its shape also recalls that of a stress-strain curve. If the cube was blocked on the sheet as supposed during the test, constraining it due to the previous hypothesis, then the load cell would read the force the material is opposing to the strain rate applied externally, giving that characteristic shape with the maximum of the curve corresponding to the point when necking occurred. Interestingly, the other coefficients measured for dry sliding with this testing configuration are in accordance with those measured by Das et al. [22].

The Cof is quite constant during sliding, as observed by Liu et al. [34] and seems to have a low strain rate-dependency, as also evidenced in Ref. [22] with extreme values between 1.5 and 1.6 in a strain rate range between $5*10^{-3}$ to $4*10^{-2}$ $s^{-1}$. Considering lubricated sliding, the expected significant reduction in Cof is observed experimentally even with this testing configuration and is one order in magnitude lower than in dry sliding (between 0.1 and 0.15). Assessing the difference between the two conditions tested in the lubricated regime is currently out of the present work scope, but interestingly, a subtle increase in Cof is observed at $2.1*10^{-2}$ $s^{-1}$ strain rate (100 mm/min) with increasing sliding distance. As predicted by different works in literature, Cof in lubricated conditions might not be constant during forming due to a reduction in the lubricant layer thickness [19,26].

### 5.1. Tribolayer formation

As documented in the literature, the direct contact between aluminum sheets and cast iron in dry sliding causes severe adhesive wear mechanisms in the tribopair (Fig. 9). According to Gali [23], the Mg-rich oxide layer that forms during sheet rolling is prone to fracture during sliding, causing plastically deformed ridges. When the strain rate decreases, the cast iron cube blocks the sheet from sliding underneath, creating a tribolayer that is approximately 15 μm thick and up to 250 μm long. This layer forms behind the cube where the sheet enters the contact area. At higher strain rates, a less noticeable tribolayer is formed, and Iron traces are found on top of the wear debris, indicating a severe adhesive wear mechanism. During sliding, the strong chemical affinity between Al and Fe leads to the formation of welded joints that are sheared during sliding. If a reacted Al—Fe compound is formed, the weak bonding causes the joint to fail within the welding itself, transferring part of the material to the counterpart surface. This mechanism seems to act preferably at low strain rates, allowing more time for the welded joint to develop.

The wear process is more complex than just adhesive wear, as observed in Fig. 8d. Microstructural constituents, such as the $Al_6Mn$ intermetallics, can also contribute to the wear process as third-body abrasive agents when are trapped in the tribolayer in their original shape or after fragmentation. A mixed adhesive-abrasive wear mechanism occurs on the aluminum sheet during sliding.

When analyzing cross-sectioned lubricated samples, no oxidized tribolayers are detected (Fig. 8 e,f). Instead, a continuous layer is found on the aluminum sheet, attributed to the lubricating paint. The paint effectively prevents direct sliding between cast iron and aluminum, even at strain rates that cause the aluminum sheet to rupture in non-lubricated conditions (1.2 * 10—3 and 4.2 * 10-2 s-1).

### 5.2. Aluminum sheet surface damaging in dry sliding conditions

A comprehensive observation of the interaction between the aluminium sheet and the cast iron is visible from the top of the sheet (Fig. 9). The prolonged contact time when low strain rates are employed favours the formation of welded joints between cast iron and the aluminium alloy, acting as a barrier to strain. Such an interaction forms a macroscopic debris responsible for scratches and bulges on the formed aluminum sheet.

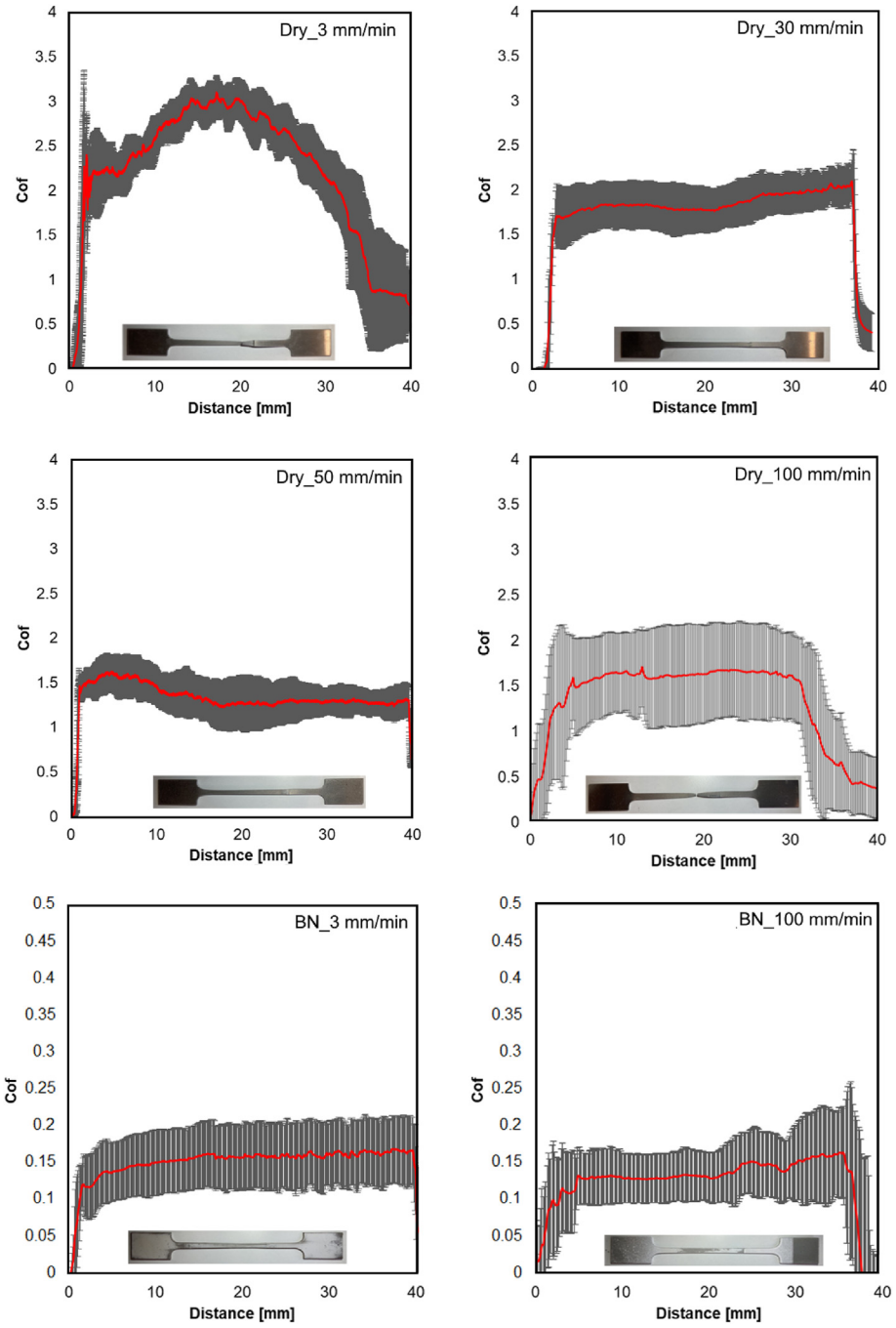


**Fig. 7.** Coefficients of friction for the different sliding conditions tested under dry and lubricated regimes.

Furthermore, coherently with the literature, the aluminium alloy flows underneath the thin superficial oxide layer that is progressively strained till rupture occurs [24] and swirl-shaped micro debris are formed.

### *5.3. Aluminum sheet surface damaging in lubricated sliding conditions*

The lubricating paint reduces the aluminium sheet's friction coefficient, scratches, and surface damage. The black areas in Fig. 10a are lubricant residues still covering the surface even after sliding. However, its relatively low hardness may be susceptible to abrasion in areas where localized high contact pressures occur near an alteration in the surface profile [35,36]. Furthermore, when the paint is abraded, the aluminium sheet is exposed to direct contact with the cast iron, resulting in isolated damage similar to that seen extensively in dry sliding conditions (as shown in Fig. 10). Therefore, as the process regards, mould polishing to reduce surface roughness below 0.1 μm has the utmost importance when manufacturing a new mould.

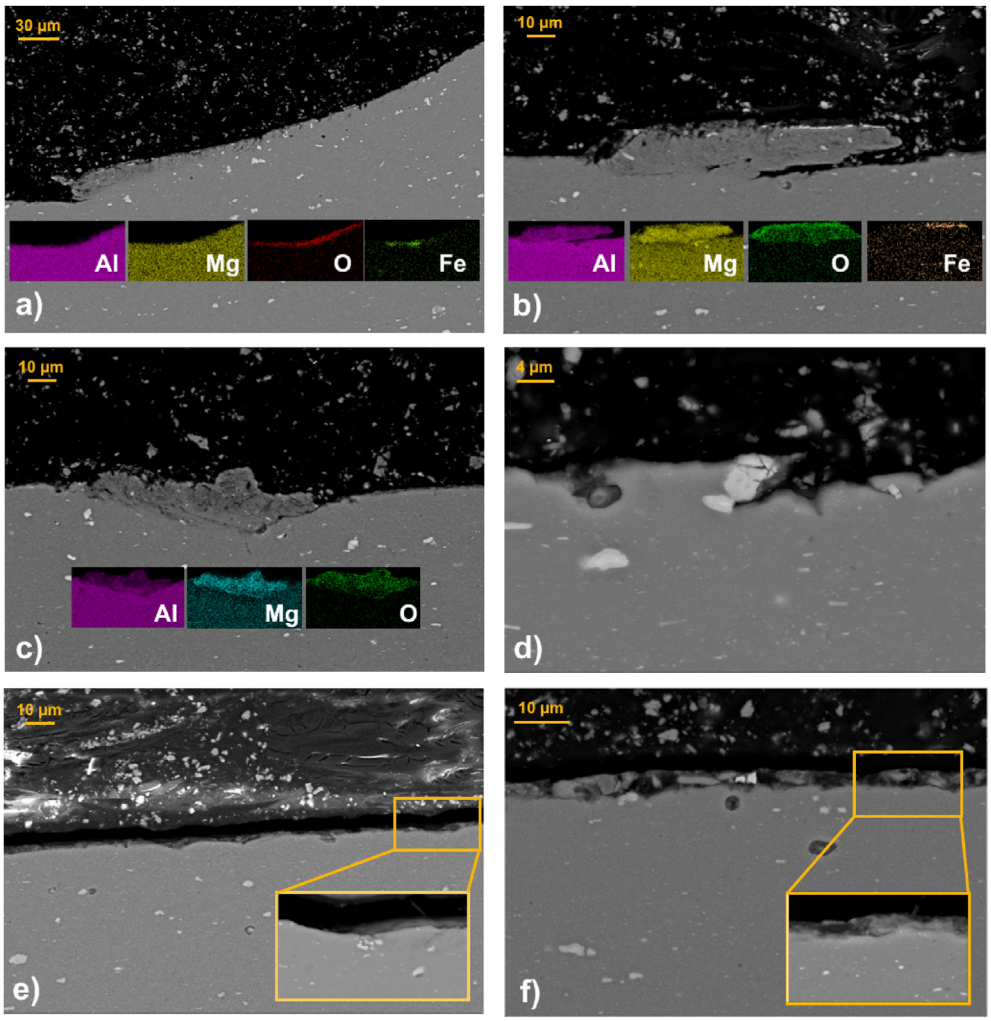


**Fig. 8.** SEM micrographs of the cross-sectioned AA 5083 samples after testing. Dry conditions strained at a) 3 mm/min, b) 30 mm/min, c) 50 mm/min, d) 100 mm/min, and lubricated at e) 3 mm/min and f) 100 mm/min.

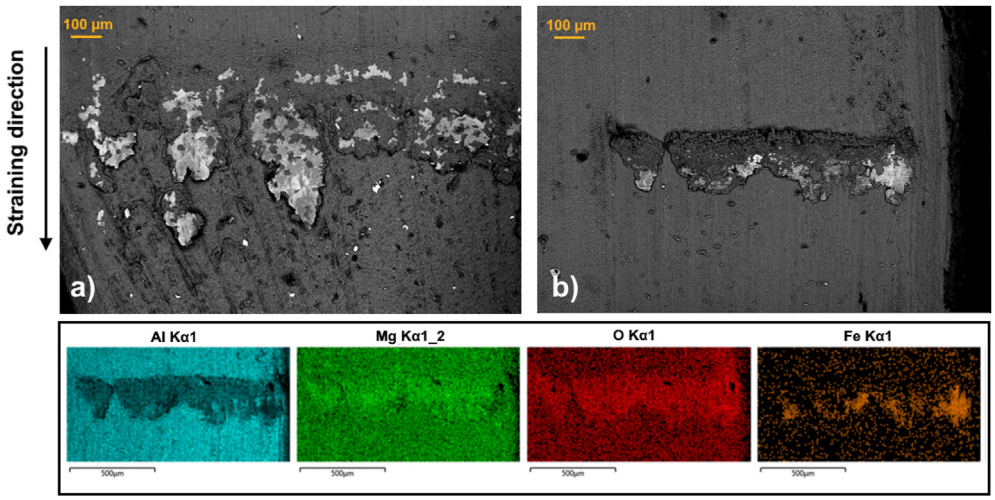


**Fig. 9.** SEM micrographs of the dry aluminium sample surface in the sliding area. a) 3 mm/min, b) 100 mm/min. Bottom part: EDS maps for the 100 mm/min sample.

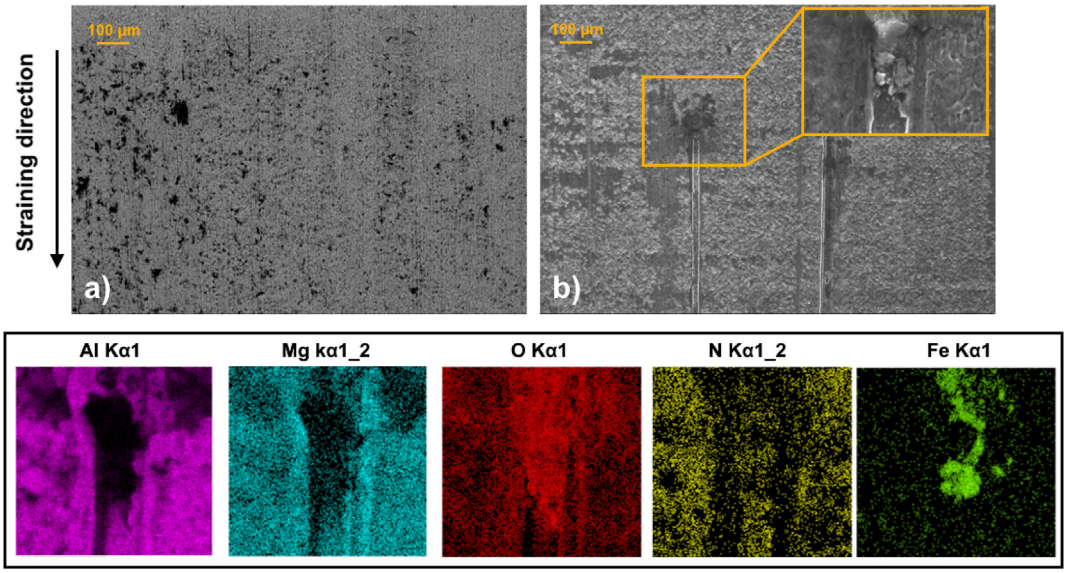


**Fig. 10.** SEM micrographs of the lubricated aluminium sample surface in the sliding area. a) 3 mm/min, b) 100 mm/min. Bottom part: EDS maps for the 100 mm/min sample.

## 6. Conclusions

This study propose a new experimental test rig to study the tribological behaviour of the aluminum – mould tribopair in superplastic forming applications. The design proposed has been validated for an AA 5083 alloy sliding against a ductile iron EN-GJS grade counterpart in dry and lubricated conditions. The main results can be summarized as follows:

- lubricant paints effectively prevented direct sliding between the aluminium sheet and cast iron, even at strain rates causing aluminium sheet rupture in non-lubricated conditions.
- In dry sliding conditions, severe adhesive wear mechanisms were observed due to the direct contact between the two materials, resulting in plastically deformed ridges, the formation of a tribolayer, and welded joints between cast iron and the aluminium alloy.
- The tribolayer formation was observed at low strain rates and acted as a barrier to strain. However, the tribolayer was less pronounced at higher strain rates, and a mixed adhesive-abrasive wear mechanism acted on the aluminium sheet during sliding.
- The aluminium sheet surface was significantly damaged in dry sliding conditions, as the alloy flowed underneath the thin superficial oxide layer that was progressively strained till rupture occurred, resulting in swirl-shaped debris formation.

The developed test rig has proven to be reliable and suitable for tribological testing, yielding comparable results while using a reduced amount of material compared to other test rigs.

## CRediT authorship contribution statement

**Federico Simone Gobber:** Writing – review & editing, Writing – original draft, Methodology, Investigation, Formal analysis, Data curation, Conceptualization. **Alexandru Tancau:** Investigation, Formal analysis. **Leonardo Daniele Scintilla:** Writing – review & editing, Project administration, Methodology, Investigation, Conceptualization. **Marco Fontana:** Supervision, Project administration, Funding acquisition. **Marco Actis Grande:** Writing – review & editing, Supervision, Project administration, Methodology, Conceptualization.

## Declaration of competing interest

The authors declare the following financial interests/personal relationships which may be considered as potential competing interests.

## Acknowledgements

A special mention is reserved to Ing. Enrico Pallavicini and Ing. Fausto Franchini for their fundamental contribution in building the test rig. The authors gratefully acknowledge the support of the Italian Ministry of Economic Development (project no. F/0150033/00/X40).

## References

[1] X. Wang, Q. Li, R. Wu, X. Zhang, L. Ma, A review on superplastic formation behavior of Al alloys, Adv. Mater. Sci. Eng. 2018 (2018) 1–17, https://doi.org/10.1155/2018/7606140.
[2] G. Luckey, P. Friedman, K. Weinmann, Design and experimental validation of a two-stage superplastic forming die, J. Mater. Process. Technol. 209 (2009) 2152–2160, https://doi.org/10.1016/j.jmatprotec.2008.05.019.
[3] J. Decrozant-Triquenaux, L. Pelcastre, B. Prakash, J. Hardell, Influence of lubrication, tool steel composition, and topography on the high temperature tribological behaviour of aluminium, Friction 9 (2021) 155–168, https://doi.org/10.1007/s40544-020-0371-6.
[4] H.Y. Wu, C.H. Chiu, J.Y. Wang, S. Lee, Effect of lubrication on deformation characteristics of a superplastic 5083 Al alloy during bi-axial deformation, Mater. Sci. Eng. 427 (2006) 268–273, https://doi.org/10.1016/j.msea.2006.04.102.
[5] P.E. Krajewski, A.T. Morales, Tribological issues during quick plastic forming, J. Mater. Eng. Perform. 13 (2004) 700–709, https://doi.org/10.1361/10599490421330.
[6] K. Mallieswaran, C. Rajendran, R. Padmanabhan, S. Rajasekaran, Evaluation of nickel shot peening process on strength of friction stir welded AA2014-T6 aluminum alloy joints, Prakt. Metallogr. Metallogr. 60 (2023) 442–460, https://doi.org/10.1515/pm-2022-1038.
[7] K. Mallieswaran, C. Rajendran, N. Aravindhan, D. Arunkumar, K. Haswanth, M. Abishek, Effect of heat treatment on the structure and properties of laser welded joints of aluminum alloy AA2024, Met. Sci. Heat Treat. 64 (2023) 564–572, https://doi.org/10.1007/s11041-023-00851-z.
[8] C. Rajendran, R. Ben Ruben, P. Ashokavarthanan, K. Mallieswaran, Identifying the effect of PWHT on strength of laser beam welding joints of AA2024 aluminum alloy, ASME Open J. Eng. 1 (2022), https://doi.org/10.1115/1.4053496.

[9] K. Mallieswaran, S. Rajasekaran, M. Vinoth Kumar, C. Rajendran, Steel shot peening effects on friction stir welded AA2014-T6 aluminum alloys, Mater. Test. 64 (2022) 1202–1213, https://doi.org/10.1515/mt-2021-2173.
[10] A.J. Barnes, Superplastic forming 40 years and still growing, J. Mater. Eng. Perform. 22 (2013) 2935–2949, https://doi.org/10.1007/s11665-013-0727-4.
[11] P.E. Krajewski, J.G. Schroth, Overview of quick plastic forming technology, Mater. Sci. Forum 551–552 (2007) 3–12, doi:10.4028/www.scientific.net/MSF.551-552.3.
[12] Y.F. Jiang, H. Ding, Investigations into hot form quench conditions on microstructure evolution and bake-hardening response for high-strength aluminum alloy, J. Mater. Eng. Perform. 29 (2020) 8331–8339, https://doi.org/10.1007/s11665-020-05245-3.
[13] K. Zheng, Y. Dong, H. Dong, J. Fernandez, T.A. Dean, Investigation of the lubrication performance using WC: C coated tool surfaces for hot stamping AA6082, Procedia Eng. 207 (2017) 711–716, https://doi.org/10.1016/j.proeng.2017.10.1046.
[14] Y. Dong, K. Zheng, J. Fernandez, G. Fuentes, X. Li, H. Dong, Tribology and hot forming performance of self-lubricious NC/NiBN and NC/WC:C hybrid composite coatings for hot forming die, J. Mater. Process. Technol. 252 (2018) 183–190, https://doi.org/10.1016/j.jmatprotec.2017.09.025.
[15] Y. Dong, K. Zheng, G. Fuentes, H. Dong, Low adhesion effect of novel duplex NC/WC:C coatings against ductile materials at elevated temperatures, Mater. Lett. 220 (2018) 32–35, https://doi.org/10.1016/j.matlet.2018.02.079.
[16] J. Decrozant-Triquenaux, L. Pelcastre, C. Courbon, B. Prakash, J. Hardell, Effect of surface engineered tool steel and lubrication on aluminium transfer at high temperature, Wear 477 (2021), https://doi.org/10.1016/j.wear.2021.203879.
[17] Y. Liu, B. Zhu, K. Wang, S. Li, Y. Zhang, Friction behaviors of 6061 aluminum alloy sheets in hot stamping under dry and lubricated conditions based on hot strip drawing test, Tribol. Int. 151 (2020) 106504, https://doi.org/10.1016/j.triboint.2020.106504.
[18] F. Jarrar, D. Sorgente, S.A. Aksenov, F. Enikeev, On the challenges and prospects of the superplastic forming process, Mater. Sci. Forum 941 (2018) 2343–2348, 10.4028/www.scientific.net/MSF.941.2343.
[19] M.D. Hanna, Tribological evaluation of aluminum and magnesium sheet forming at high temperatures, Wear 267 (2009) 1046–1050, https://doi.org/10.1016/j.wear.2009.01.007.
[20] P.A. Friedman, S.G. Luckey, W.B. Copple, R. Allor, C.E. Miller, C. Young, Overview of superplastic forming research at ford motor company, J. Mater. Eng. Perform. 13 (2004) 670–677, https://doi.org/10.1361/10599490421277.
[21] B. Rodríguez Leal, J. Decrozant-Triquenaux, J. Hardell, L. Pelcastre, Development of a laboratory-scale test methodology for performance evaluation of lubricants for hot stamping of an aluminium alloy, Lubricants 11 (2023), https://doi.org/10.3390/lubricants11090359.
[22] S. Das, A.T. Morales, A.R. Riahi, X. Meng-Burany, A.T. Alpas, Role of plastic deformation on elevated temperature tribological behavior of an Al-Mg alloy (AA5083): a friction mapping approach, Metall. Mater. Trans. A 42 (2011) 2384–2401, https://doi.org/10.1007/s11661-011-0649-4.
[23] O.A. Gali, A.R. Riahi, A.T. Alpas, The tribological behaviour of AA5083 alloy plastically deformed at warm forming temperatures, Wear 302 (2013) 1257–1267, https://doi.org/10.1016/j.wear.2012.12.048.
[24] O.A. Gali, A.R. Riahi, A.T. Alpas, The effect of surface conditions on the elevated temperature sliding contact deformation of AA5083 alloy, Wear 330–331 (2015) 309–319, https://doi.org/10.1016/j.wear.2014.12.027.
[25] Z. Chen, P.F. Thomson, Friction against superplastic aluminium alloys, Wear 201 (1996) 227–232, https://doi.org/10.1016/S0043-1648(96)07254-7.
[26] D. Sorgente, A. Lombardi, D. Coviello, L.D. Scintilla, M. Fontana, A strain-dependent model for the coefficient of friction in the tool-blank interaction in superplastic forming, J. Manuf. Process. 73 (2022) 791–798, https://doi.org/10.1016/j.jmapro.2021.11.050.
[27] P.A. Friedman, S.G. Luckey, High-temperature lubricants for superplastic forming of metals, Superplast. Form. Adv. Met. Mater. (2011) 72–82, https://doi.org/10.1533/9780857092779.1.72.
[28] ASTM E407-07 - Standard Practice for Microetching Metals and Alloys.
[29] Z. Zeng, Y. Zhang, Y. Zhou, Q. Jin, Superplastic forming of aluminum alloy car body panels, Mater. Sci. Forum 475–479 (2005) 3025–3028, https://doi.org/10.4028/0-87849-960-1.3025.
[30] P.E. Krajewski, J.G. Schroth, Overview of quick plastic forming technology, Mater. Sci. Forum 551–552 (2007) 3–12, https://doi.org/10.4028/0-87849-435-9.3.
[31] P. He, D. Liu, Mechanism of forming interfacial intermetallic compounds at interface for solid state diffusion bonding of dissimilar materials, Mater. Sci. Eng. 437 (2006) 430–435, https://doi.org/10.1016/j.msea.2006.08.019.
[32] Y. Hu, Y. Zheng, D.J. Politis, M.A. Masen, J. Cui, L. Wang, Development of an interactive friction model to predict aluminum transfer in a pin-on-disc sliding system, Tribol. Int. 130 (2019) 216–228, https://doi.org/10.1016/j.triboint.2018.08.034.
[33] O. El Fakir, L. Wang, D. Balint, J.P. Dear, J. Lin, T.A. Dean, Numerical study of the solution heat treatment, forming, and in-die quenching (HFQ) process on AA5754, Int. J. Mach. Tool Manufact. 87 (2014) 39–48, https://doi.org/10.1016/j.ijmachtools.2014.07.008.
[34] Y. Liu, Z. Zhu, Z. Wang, B. Zhu, Y. Wang, Y. Zhang, Flow and friction behaviors of 6061 aluminum alloy at elevated temperatures and hot stamping of a B-pillar, Int. J. Adv. Manuf. Technol. 96 (2018) 4063–4083, https://doi.org/10.1007/s00170-018-1790-7.
[35] J. Eichler, K. Uibel, C. Lesniak, Boron nitride (BN) and boron nitride composites for applications under extreme conditions, 12th Int. Ceram. Congr. PART D 65 (2010) 61–69, 10.4028/www.scientific.net/ast.65.61.
[36] J. Heinrichs, S. Jacobson, The influence from shape and size of tool surface defects on the occurrence of galling in cold forming of aluminium, Wear 271 (2011) 2517–2524, https://doi.org/10.1016/j.wear.2011.01.077.